Universidade Federal de Juiz de Fora
Instituto de Ciências Exatas
Bacharelado em Ciência da Computação

Implementation and Evaluation of Differential Optical Flow Methods

Luciano Walenty Xavier Cejnog

JUIZ DE FORA
AGOSTO, 2013

Implementation and Evaluation of Differential Optical Flow Methods

Luciano Walenty Xavier Cejnog

Universidade Federal de Juiz de Fora

Instituto de Ciências Exatas

Departamento de Ciência da Computação

Bacharelado em Ciência da Computação

Orientador: Marcelo Bernardes Vieira

JUIZ DE FORA

AGOSTO, 2013

Implementation and Evaluation of Differential Optical Flow Methods

Luciano Walenty Xavier Cejnog

MONOGRAFIA SUBMETIDA AO CORPO DOCENTE DO INSTITUTO DE CIÊNCIAS EXATAS DA UNIVERSIDADE FEDERAL DE JUIZ DE FORA, COMO PARTE INTEGRANTE DOS REQUISITOS NECESSÁRIOS PARA A OBTENÇÃO DO GRAU DE BACHAREL EM CIÊNCIA DA COMPUTAÇÃO.

Aprovada por:

Marcelo Bernardes Vieira
Doutor em Ciência da Computação

Rodrigo Luís de Souza da Silva
Doutor em Engenharia Civil

Saul de Castro Leite
Doutor em Modelagem Computacional

JUIZ DE FORA

29 DE AGOSTO, 2013

For my parents, my brothers and my friends.

Resumo

Este trabalho busca realizar uma análise comparativa de três métodos de determinação de fluxo óptico entre imagens: os tradicionais métodos de Lucas-Kanade e Horn-Schunck e o método de Augereau. Para tal análise, são introduzidos conceitos de dinâmica dos fluidos. O trabalho apresenta os métodos fazendo uma analogia entre o processo de determinação do fluxo óptico e o processo de difusão de fluidos.

Palavras-chave: Fluxo óptico, dinâmica dos fluidos, Navier-Stokes equations.

Abstract

This work aims to realize a comparative analysis of three optical flow determination techniques: the traditional Lucas-Kanade and Horn-Schunck methods and the recent Augereau method. This work evaluates the methods on fluid dynamics viewpoint, making an analogy between optical flow determination and fluid diffusion process.

Keywords: Optical flow, fluid dynamics, Navier-Stokes equations.

Thanks

For all my relatives, for constant encouragement and support.

For my friends on UFJF, GCG and GETComp, and my classmates.

For the teachers of Computer Science Department on UFJF for all the lessons, and for all those who somehow helped me getting more knowledge and professional enrichment.

For the people on COPESE, CAE, IF-Sudeste-MG, and all the places I had the opportunity to work, which also contributed on my formation.

Contents

List of Figures

List of Tables

"Go back?" he thought. "No good at all! Go sideways? Impossible! Go forward? Only thing to do! On we go!" So up he got, and trotted along with his little sword held in front of him and one hand feeling the wall, and his heart all of a patter and a pitter.

J. R. R. Tolkien (The Hobbit)

1 Introduction

Movement detection on image streams is a core field of computer vision. Various applications arise from this task. The estimated field of velocities which describes movement on an image is named *optical flow*. Several methods estimate local optical flow by using a simplified version of Navier-Stokes equations.

The determination of optical flow comes from assuming that between two frames the intensity of a pixel does not change, although its position can vary. This constraint is insufficient to grant reliability of solutions. This way, for the computation of optical flow, it is necessary to determine other constraints, called *contour constraints* [16].

Different methods were proposed to estimate optical flow, using different contour constraints. Literature classifies methods into three main approach types: differential methods, phase-based methods and correlation methods. Some methods use feature extraction to reduce the amount of processing. The main focus of this work is on differential methods.

This work has two main purposes: to present fluid dynamics concepts associated to optical flow estimation, and to analyze three differential approaches of optical flow, analyzing their errors in detecting ground-truth optical flows. Two of them are classical methods largely known and explored by literature - Horn and Schunck and Lucas-Kanade. The third is Augereau method, a more recent approach, based on the use of orientation tensors.

The next chapters are divided as follows: Chapter two presents the theoretical basis with the fundamentals of fluid dynamics and mathematical description of the optical flow methods. Chapter three deals with the computational model used and some details on implementation of the methods. Chapter four presents an analysis of the ground-truth images results, and the fifth chapter brings the conclusion and future works.

1.1 Problem definition

The main problem discussed on this work is the computation of optical flow between two consecutive frames in a video I_1 and I_2. It is composed by the velocity vector field $V(x, y) = [u(x, y), v(x, y)]$ for each pixel (x, y) on image I_1 that indicates its correspondent pixel on image I_2. Ideally, the optical flow represents the motion of the objects represented on both frames.

1.2 Objectives

This work's main objective is the study and implementation of optical flow estimation methods. The secondary objectives are:

- To associate flow dynamics elements to the basic concepts of the methods,
- To test and evaluate results of optical flow estimation for ground-truth images,
- To present implementation details of each method,
- To compare results on the implementation of optical flow methods.

2 Theoretical basis

This chapter presents the theoretical basis of the work, which includes notions of kinematics and fluid dynamics, the mathematical definition of optical flow, and a brief presentation of variants on optical flow estimation methods.

2.1 Kinematics and Fluid Dynamics

2.1.1 Basic Concepts

This section describes basic concepts in fluid dynamics: fluid flow and rate of change following a fluid. Yet, the notion of an ideal fluid is introduced. This concept is necessary for the domain definition of Navier-Stokes equation, which will be discussed in the next section. All the concepts defined in this section are based on [1].

Definition 2.1.1. (Fluid Flow) The fluid flow is usually defined as the set of vectors $\vec{u} : (\mathbb{R}^n, \mathbb{R}) \to \mathbb{R}^n$ which specifies flow velocity for each point of the flow $\vec{x} \in \mathbb{R}^n$ in time $t \in \mathbb{R}$. As example, a three-dimensional flow can be written as $\vec{u} = [u(x, y, z, t)$, $v(x, y, z, t)$, $w(x, y, z, t)$, $t]$.

Definition 2.1.2. (Streamline) Considering a three-dimensional flow field, a streamline can be defined as the set of points $\vec{x} = [x(s), y(s), z(s)]$ where s denotes distance along a streamline, and the following condition is satisfied:

$$\frac{dx/ds}{u} = \frac{dy/ds}{v} = \frac{dz/ds}{w}.$$

The set of points on a streamline defines a curve where flow field has the same direction.

Definition 2.1.3. (Rate of Change) Let $f(x, y, z, t)$ denote a quantity of interest in the fluid motion. The rate of change of f following the fluid is defined as $\frac{Df}{Dt}$:

$$\frac{Df}{Dt} = \frac{\mathrm{d}}{\mathrm{d}t} f(x(t), y(t), z(t), t),$$

$$\frac{Df}{Dt} = u\frac{\partial f}{\partial x} + v\frac{\partial f}{\partial y} + w\frac{\partial f}{\partial z} + \frac{\partial f}{\partial t}.$$

On the equation above, $x(t)$, $y(t)$ and $z(t)$ change with time according to the local field velocity $\vec{u}$.

$$\vec{u} = [u, v, w], \begin{cases} \frac{\mathrm{d}x}{\mathrm{d}t} = u, \\ \frac{\mathrm{d}y}{\mathrm{d}t} = v, \\ \frac{\mathrm{d}z}{\mathrm{d}t} = w. \end{cases}$$

The notation $\frac{Df}{Dt}$ indicates a material derivative, which is a way to describe the local spatio-temporal rate of change of an element in a fluid. The local rate of change of f can, so, be written in terms of the local field velocity, by the following relation:

$$\frac{Df}{Dt} = \frac{\partial f}{\partial t} + (\vec{u} \cdot \nabla f),$$

where $\vec{u} = [u, v, w]$.

By deriving the above equation, it is possible to define $\frac{D\vec{u}}{Dt}$ as the local field acceleration of an element:

$$\frac{D\vec{u}}{Dt} = \frac{\partial u}{\partial t} + (\vec{u} \cdot \nabla u)\vec{u}.$$

With the definition of rate of change, it is possible to prove that the following statements are true:

1. The scalar product $\vec{u} \cdot \nabla f$ is equivalent to $|\vec{u}|\frac{\partial f}{\partial s}$,
2. If $\vec{u} \cdot \nabla f = 0$, f is constant along a streamline,
3. If $\frac{Df}{Dt} = 0$, f is constant for a particular fluid element.

Some theoretical studies about fluid dynamics are only possible considering some properties. It was necessary to establish certain constraints to study some useful properties. Those constraints yielded to ideal fluid definition.

Definition 2.1.4. (Ideal Fluid) An ideal fluid satisfies the following properties:

1. It is incompressible, which implies that rate of change of its volume on time is zero,

2. Its density ρ is constant,

3. The force exerted across a geometrical element $\vec{n} \cdot \delta S$ within the fluid is $p \cdot \vec{n} \cdot \delta S$, where $p(x, y, z, t)$ is a scalar function independent of the normal $\vec{n}$, called pressure.

2.1.2 Navier-Stokes Diffusion Equation

This section presents a brief background on fluid dynamics and development of Navier-Stokes equations. For further detail, see [1].

In Book II of the *Principia* (1687), Isaac Newton tried to describe the circular motion of fluids. Although it was a good starting point to fluid mechanics theory, his hypothesis could lead to wrong assumptions over the mathematical relationship between radius and angular velocity. Quoting [1], "this error gives one small indication of how rudimentary fluid mechanics was at the time, even in the hands of a great master".

John Bernoulli described the concept of internal pressure in 1743, on *Hydraulica*. Furthermore, the basic principles of mechanics arose with Euler at 1752, with the principle of linear momentum. In 1755, Euler combined Bernoulli's internal pressure with the principle of linear momentum and obtained motion equations for an inviscid fluid.

Definition 2.1.5. (Euler's Equations) Euler's equations described movement on an ideal fluid. On the following equations, term p represents fluid pressure; g is gravitational body force per mass, $\vec{u} = [u, v, w]$ is the local velocity vector and ρ is the density of the fluid.

$$
\begin{aligned}
\frac{\partial u}{\partial t} + u\frac{\partial u}{\partial x} + v\frac{\partial u}{\partial y} + w\frac{\partial u}{\partial z} &= -\frac{1}{\rho} \cdot \frac{\partial p}{\partial x}, \\
\frac{\partial v}{\partial t} + u\frac{\partial v}{\partial x} + v\frac{\partial v}{\partial y} + w\frac{\partial v}{\partial z} &= -\frac{1}{\rho} \cdot \frac{\partial p}{\partial y}, \\
\frac{\partial w}{\partial t} + u\frac{\partial w}{\partial x} + v\frac{\partial w}{\partial y} + w\frac{\partial w}{\partial z} &= -\frac{1}{\rho} \cdot \frac{\partial p}{\partial z} - g, \\
\frac{\partial u}{\partial x} + \frac{\partial v}{\partial y} + \frac{\partial w}{\partial z} &= 0.
\end{aligned}
$$

The next step in fluid dynamics equations was given by Cauchy in 1822, when he introduced *stress tensor* concept.

Definition 2.1.6. (Stress Tensor) Let $\vec{x}$ denote the position vector of some fixed point on the fluid, and δS be a small geometrical surface element, with unit normal vector $\vec{n}$. The stress tensor for point $\vec{x}$ is defined by a 3×3 matrix for which each element $(\mathbf{T})_{ij}$ is the i-th component of stress on a surface element δS which has a normal $\vec{n}$ pointing in j-th direction.

With the stress tensor, it is possible to define the force $\vec{F}$ exerted on this surface by the fluid towards which n is directed. It is defined as:

$$\vec{F} = \vec{t} \cdot \delta S,$$

where $\vec{t}$ is named stress vector. It can be proved that the stress vector can be expressed in terms of stress tensor and of the component j of the normals, using the following relation:

$$\vec{t} = (\mathbf{T}) \cdot \vec{n}^T.$$

Using notion of the stress tensor, Cauchy was able to define a general equation of motion for any continuous medium:

$$\rho \cdot \frac{Du_i}{Dt} = \frac{\partial (\mathbf{T})_{ij}}{\partial x_j} + \rho g_i. \tag{2.1}$$

This is obtained considering the i-th component of force exerted by the surrounding fluid on an infinitesimal part of surface S:

$$\int_S t_i dS = \int_S (\mathbf{T})_{ij} \cdot n_j dS = \int_V \frac{\partial (\mathbf{T})_{ij}}{\partial x_j} dV.$$

An algebraic way to obtain the Cauchy Equation is by using Reynolds's transport theorem, that states:

Theorem 2.1.1. *Reynolds's transport theorem*

$$\frac{\mathrm{d}}{\mathrm{d}t} \int_{V(t)} G \cdot dV = \int_{V(t)} \frac{DG}{Dt} + G \nabla \cdot u,$$

where $G(x,t)$ is any scalar or vector function and $V(t)$ denotes the region of space occupied *by an infinitesimal part of the fluid.*

Finally, Navier and Stokes related Cauchy's stress tensor concept with the previous results.

If the fluid's density is ρ and its viscosity is μ, it is possible to obtain numerical values for the stress tensor in function of ρ, μ and the flow variables.

$$(\mathbf{T})_{ij} = -p\delta_{ij} + \mu\Big(\frac{\partial u_j}{\partial x_i} + \frac{\partial u_i}{\partial x_j}\Big). \tag{2.2}$$

On the Equation 2.2, δ_{ij} is the Kronecker's Delta, defined by:

$$\delta_{ij} = \begin{cases} 1, \text{ if } i = j, \\ 0, \text{ if } i \neq j. \end{cases}$$

Notably, stress tensor is symmetric, reducing the amount of equations to six. In case of constant viscosity μ, it is possible to substitute terms of Equation 2.2 in Equation 2.1, writing:

$$\rho\frac{Du_i}{Dt} = -\frac{\partial p}{\partial \vec{x}_i} + \mu\frac{\partial}{\partial \vec{x}_j}\Big(\frac{\partial u_j}{\partial \vec{x}_i} + \frac{\partial u_i}{\partial \vec{x}_j}\Big) + \rho g_i,$$

$$\rho\frac{Du_i}{Dt} = -\frac{\partial p}{\partial \vec{x}_i} + \mu\frac{\partial}{\partial \vec{x}_i}\frac{\partial u_j}{\partial \vec{x}_j} + \mu\frac{\partial^2 u_i}{\partial^2 \vec{x}_j} + \rho g_i.$$

But $\vec{x}_j = [x_1, x_2, x_3]$, so we can write:

$$\frac{\partial^2}{\partial \vec{x}_j^2} = \frac{\partial^2}{\partial x_1^2} + \frac{\partial^2}{\partial x_2^2} + \frac{\partial^2}{\partial x_3^2}.$$

The pressure of a fluid is defined in terms of the stress tensor is:

$$p = -\frac{1}{3}(T_{11} + T_{22} + T_{33}).$$

Also, we define v as the kinematic viscosity of the fluid. The value of v is obtained by:

$$v = \frac{\mu}{\rho}$$

With the fundamentals above, it is possible to define Navier-Stokes equation.

Definition 2.1.7. (Navier-Stokes Equation) For a viscous fluid, the Navier-Stokes equation is:

$$\frac{\partial u}{\partial t} + (\vec{u} \cdot \nabla)\vec{u} = -\frac{1}{\rho}\nabla p + v\nabla^2\vec{u} + \vec{g}, \tag{2.3}$$

This Navier-Stokes equation represents the process of diffusion and advection of an incompressible fluid flow. The term $v\nabla^2\vec{u}$ represents diffusion, and $(\vec{u} \cdot \nabla)\vec{u}$ is the corresponding term for advection.

In fluid dynamics simulating applications usually the fluid is considered incompressible, so that constraint $\nabla \cdot \vec{u} = 0$ is applied. This simplifies the amount of computation.

2.2 Optical Flow

Definition 2.2.1. (Optical Flow) *Optical flow* is the pattern of apparent motion of objects, surfaces and edges caused by relative motion between an observer and a camera. In video processing, determining optical flow corresponds to determine the velocity field which describes each pixel's movement.

Let $I(x, y, t)$ be the brightness intensity function of a point (x, y) in the frame number t of an image stream. We assume that in a small time interval an object can change its position, although its reflectivity and illumination will not vary, which can be represented by the following equation:

$$I(x + \Delta x, y + \Delta y, t + \Delta t) \approx I(x, y, t).$$

Assuming that this constraint is complied is equivalent to consider that all pixels on the frame t will remain intact on the image in the frame $t + \Delta t$ and will not change its brightness. This is a strong assumption for real cases. The error associated for optical flow measurement on real sequences of images tends to be high, since there is no guarantee that pixels will not be created or destroyed at each frame.

Expanding the equation by Taylor series:

$$I(x+\Delta x, y+\Delta y, t+\Delta t) = I(x,y,t) + \frac{\partial I}{\partial x}\Delta x + \frac{\partial I}{\partial y}\Delta y + \frac{\partial I}{\partial t}\Delta t + h.o.t.$$

Ignoring higher-order terms, the above equation can only be assumed as true if the following constraint is satisfied:

$$\frac{\partial I}{\partial x}\Delta x + \frac{\partial I}{\partial y}\Delta y + \frac{\partial I}{\partial t}\Delta t = 0.$$

Considering $\Delta t = 1$, we obtain the main optical flow constraint:

$$\nabla I \cdot \vec{v} + I_t = 0. \qquad (2.4)$$

On the above equation, $\nabla I = \left[\frac{\partial I}{\partial x}, \frac{\partial I}{\partial y}\right]$ is the spatial gradient, $\vec{v} = [u, v] = [\Delta x, \Delta y]$ is the optical flow vector, and I_t is the partial derivative from the brightness intensity function on time.

2.2.1 Physical comparison

There is an analogy that can be made between optical flow vector field and fluid equations of motion. It is possible to consider an image as a bidimensional fluid varying in time. In that case, the main optical flow constraint (Equation 2.4) indicates that in an exact process there is no addition to original flow content, although particles' position vary inside the field through time. This indicates an incompressible flow. Therefore, Navier-Stokes' equations are used as a basis to optical flow determination.

As a fluid simulation process, optical flow is considered a process with dominant convective phenomena. The equations are simplified by disconsidering the diffusion term $v\nabla^2\vec{u}$, the external force term $\vec{g}$, and the internal pressure term $-\frac{1}{\rho}\nabla p$.

Of course the choice of considering incompressible flow changes the landscape of the problem. The solution obtained will be not exact in most cases, because pixels will often be created and destroyed at each frame. Some approaches [27] propose alternatives to this constraint, assuming high correlation between images. Another problem caused by the main optical flow constraint is about the continuity of time domain. Navier-Stokes process consider continuous time, while the time in optical flow field calculation is assumed to be discretized, since the frame set used on estimative is not continuous.

2.2.2 The aperture problem

By considering only the main optical flow constraint, optical flow estimation can compute the component of the movement in the direction of the spatial gradient. But this constraint alone is unable to estimate correctly other components of the field. This causes a problem in the process, known as the aperture problem.

This problem accentuates in regions of homogeneous brightness, where the gradient of the image is null. In these regions, any point on the neighborhood could be the corresponding point on the other image. Therefore optical flow measurement becomes ambiguous, and this constraint is insufficient.

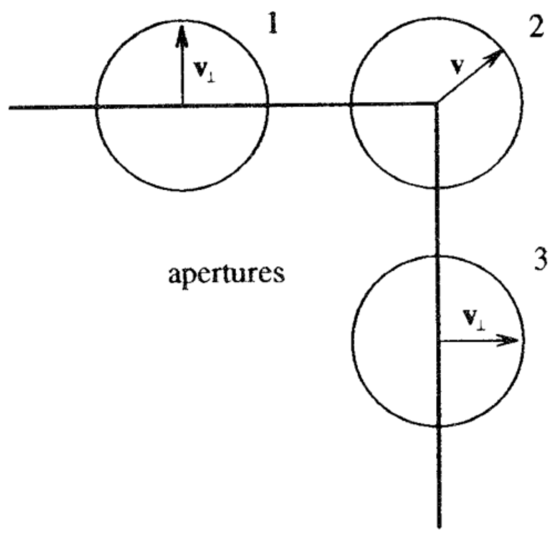

Figure 2.1: Aperture problem example [9].

Figure 2.1 illustrates the aperture problem. Along the edges, optical flow represents only the motion on direction of normal vector. On the corner (2), there is sufficient local gradient information, so optical flow vector represents correctly the measurement of motion.

2.2.3 General unidimensional movement

To measure optical flow between two signals $G(\vec{x})$ and $F(\vec{x})$ is to obtain the displacement vector $\vec{h}$ such as $F(\vec{x}+\vec{h}) = G(\vec{x})$.

The work of Lucas and Kanade [20] defines forms of measuring error between $G(\vec{x})$ and $F(\vec{x}+\vec{h})$ on a region of interest R:

- L_1-norm: $\sum_{x\in R} |F(\vec{x}+\vec{h}) - G(\vec{x})|$,
- L_2-norm: $\sqrt{\sum_{x\in R} |F(\vec{x}+\vec{h}) - G(\vec{x})|^2}$,
- Negative of normalized correlation: $\dfrac{\sum_{\vec{x}\in R} -F(\vec{x}+\vec{h})\cdot G(\vec{x})}{\sqrt{\sum_{\vec{x}\in R} F(\vec{x}+\vec{h})^2}\cdot\sqrt{\sum_{\vec{x}\in R} G(\vec{x})^2}}$.

Considering an one-dimensional case, it is possible to determine an approximation to optical flow in function of displacement h between two signals $F(x)$ and $G(x)$, by considering $G(x) = F(x+h)$. This development is detailed on Lucas and Kanade's approach.

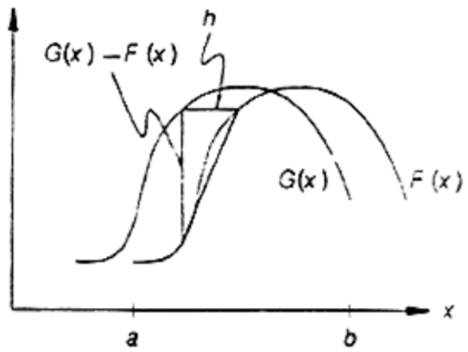

Figure 2.2: One-dimensional functions $F(x)$ and $G(x)$ with displacement h [20].

Taking a limit of the equation when h tends to 0, we obtain the spatial derivative:

$$\lim_{h\to 0} \frac{F(x+h) - F(x)}{h} \approx \frac{\partial F}{\partial x}.$$

Considering time displacement between signals $\Delta t = 1$, it is also possible to obtain an approximate measurement of temporal derivative $\frac{\partial F}{\partial t}$ as:

$$\frac{\partial F}{\partial t} = F(x+h) - F(x).$$

Relating spatial and temporal derivatives, we obtain:

$$\frac{\partial F}{\partial t} = \frac{\partial F}{\partial x} \cdot h.$$

Intuitively, this term is a simplificed version of optical flow main constraint (Equation 2.4). On relating this equation to the original constraint, we can consider:

$$\begin{cases} \nabla I = \frac{dF}{dx}, \\ \vec{v} = h, \\ I_t = \frac{dF}{dt}. \end{cases}$$

That confirms that for small values of displacement h, the main optical flow constraint is capable to represent rigid movement.

2.3 Optical Flow Approaches

Based on the aperture problem, it becomes necessary to define contour constraints, which is a new set of constraints to be applied so that the process can be done not only in the gradient direction.

This necessity yielded several approaches based on different sets of restrictions. According to Barron and Beauchemin [8], those approaches can be classified as:

- Differential methods: create constraints based on spatio-temporal derivatives of image brightness or consider filtered versions of the images. These approaches can be classified as global or local, depending on the amount of information used to estimate optical flow. The methods of Horn and Schunck [16], Lucas and Kanade [20] and Nagel [24] are examples of differential methods.

- Region-based matching methods: based on similarity measures between the neighborhood of pixels in the first image and candidate pixels in the second. These methods are less sensitive to noise compared to differential methods. However, they are far more expensive, considering the number of comparisons needed. Some methods are used together with feature extraction techniques, which reduces its computational cost. Anandan et al [2] is an example of a region-based hierarchical method.

- Energy-Based methods: based on energy of velocity-tuned filters. Some methods on this class are based on Fourier domain. An example to this class of methods is Heeger [15].

- Phase based methods: Defines velocity as phase of band-pass filter outputs. Examples are Waxman et al [33] and Fleet and Jepsen [12], which is one of the recommended methods on Barron's review.

The focus of this work is on differential methods, due to their efficiency on performance and reasonably good precision. Some applications of optical flow, such as building a descriptor for motion in videos [23] use this kind of approach. We will now introduce mathematical model of three differential methods: the classical approaches of Horn and Schunck (global differential), Lucas and Kanade (local differential), and the relatively new Augereau's formulation.

2.3.1 Horn and Schunck

Horn and Schunck method [16] is a differential global method. This method was one of the first optical flow estimative approaches proposed. This way, Horn and Schunck's work was largely cited and explored in literature, and several approaches are based on this method.

Horn and Schunck's approach tries to solve the aperture problem by considering that the optical flow field varies smoothly through the entire image. The method is based on error minimization of the following function:

$$E^2 = \int\int \nabla I \cdot v + I_t + \alpha^2 \left(\frac{\partial u}{\partial x}^2 + \frac{\partial u}{\partial y}^2 + \frac{\partial v}{\partial x}^2 + \frac{\partial v}{\partial y}^2 \right) dxdy. \tag{2.5}$$

The error to be minimized considers a weighted sum of optical flow's main constraint and a smoothness constraint, defined by:

$$E_c^2 = \frac{\partial u}{\partial x}^2 + \frac{\partial u}{\partial y}^2 + \frac{\partial v}{\partial x}^2 + \frac{\partial v}{\partial y}^2 .$$

Helmholtz theorem states that any static vector field can be decomposed in two components: an irrotational (curl-free) component and a solenoidal (divergent-free) component. Recently, it has been proved by [14] that the error function adopted by Horn and Schunck corresponds to an equal penalty on divergence and curl of the vector field.

It is clear that Horn and Schunck approach's smoothness constraint generates problems to deal with discontinuities on images. On frames with rough movement, the estimative tends to be highly inaccurate. Of course, this is a major problem of all differential methods. As an advantage, the flow vector field resulted of this method is more dense if compared to the result of local approaches.

2.3.2 Lucas-Kanade

Lucas and Kanade approach [20] is a differential local method. This method solves optical flow by considering a weighted window around each pixel, and makes least-squares fit.

Lucas and Kanade assume that in a small neighborhood the flow is smooth. Therefore, considering the general equations described on Section 2.2.2, the value of the displacement could be computed by using an average process:

$$h \approx \frac{\sum_{x\in\Omega} \frac{G(x)-F(x)}{F'(x)}}{\sum_{x\in\Omega} 1}$$

But this approximation can be improved, since the closer points in the neighborhood generates more precise values of $\frac{\partial F}{\partial x}$. Therefore, the approach combines the various estimates of h at various values of x by making a weighted sum of derivatives in a small neighborhood:

$$h \approx \frac{\sum_{x\in\Omega} \frac{w(x)(G(x)-F(x))}{F'(x)}}{\sum_{x\in\Omega} w(x)}. \tag{2.6}$$

This constraint then is generalized for a displacement on higher dimensions, by considering

$$F(\vec{x}+h) = F(\vec{x}) + h\frac{\partial}{\partial \vec{x}}F(x),$$

with $\frac{\partial}{\partial \vec{x}} = \sum_i \frac{\partial}{\partial x_i}$.

In this case, the term to be minimized is

$$h = \Big[\sum_{\vec{x}\in\Omega} \Big(\frac{\partial F}{\partial \vec{x}}\Big)^T \cdot [G(\vec{x}) - F(\vec{x})]\Big] \cdot \Big[\sum_{\vec{x}\in\Omega} \Big(\frac{\partial F}{\partial \vec{x}}\Big)^T \cdot \Big(\frac{\partial F}{\partial \vec{x}}\Big)\Big]^{-1}.$$

Typically, the weighting mask used is a gaussian mask of independent size, variating with the amount of neighbour elements desired for the process of the flow computation.

Extending the solution for the image domain, the error function to be minimized by Lucas and Kanade is then defined by:

$$E_{LK} = \sum_{\vec{x}\in\Omega} w^2(\vec{x}) \cdot \Big(\nabla I(\vec{x}, t) \cdot \vec{v} + \frac{\partial I}{\partial t}\Big). \tag{2.7}$$

The final solution is given by considering a linear system of size of the neighborhood for each pixel. The main advantage of the local differential displacement minimization, in comparision to global Horn and Schunck method, is the reduced sensitivity to discontinuities on flow, for considering the variation over the weighted window. This way, variations on parts of the image will not influence distant pixels.

2.3.3 Augereau

Augereau et al [4] addresses the problem of the computation of optical flow on multi-band image sequences. The brightness on the image I is now described by a three-dimensional vector $\vec{I} = [I_1, I_2, I_3]$. For each dimension on color space, it is possible to compute a vector field.

Therefore, the problem is to find a vector field capable of describe the resulting flow on color images. By expressing optical flow main constraint (Equation 2.4) for each dimension, we obtain:

$$\begin{aligned} \tfrac{\partial I_1}{\partial x} u + \tfrac{\partial I_1}{\partial y} v + \tfrac{\partial I_1}{\partial t} &= 0, \\ \tfrac{\partial I_2}{\partial x} u + \tfrac{\partial I_2}{\partial y} v + \tfrac{\partial I_2}{\partial t} &= 0, \\ \tfrac{\partial I_3}{\partial x} u + \tfrac{\partial I_3}{\partial y} v + \tfrac{\partial I_3}{\partial t} &= 0. \end{aligned}$$

This linear system is overdeterminated, and three main strategies were developed: to select two equations in order to obtain a direct estimation [22, 25], to solve the system using least squares [7, 13, 25, 38], or to fuse the results on flow to recover one vector field [3]. Color optical flow vector must also be a potential optical flow vector for each dimension, and all three strategies mentioned fail to achieve this property.

Augereau's approach aims to determine an optical flow vector field which satisfies the following constraint:

$$\vec{v}^T \cdot \nabla \vec{I} = 0,$$

where $\vec{v} = [u, v, 1]$, and ∇I is the multi-band color gradient direction of the vetorial image $\vec{I}$. To ensure this, the approach defines the structure tensor of a pixel:

Definition 2.3.1. (Structure Tensor) For one brightness channel, considering the gradient vector $\nabla I^T = \left[\frac{\partial I}{\partial x}, \frac{\partial I}{\partial y}, \frac{\partial I}{\partial t}\right]$, the *structure tensor* $(\mathbf{S})$ [32] is defined by:

$$(\mathbf{S}) = \begin{bmatrix} \frac{\partial I}{\partial x}^2 & \frac{\partial I}{\partial x}\frac{\partial I}{\partial y} & \frac{\partial I}{\partial x}\frac{\partial I}{\partial t} \\ \frac{\partial I}{\partial x}\frac{\partial I}{\partial y} & \frac{\partial I}{\partial y}^2 & \frac{\partial I}{\partial y}\frac{\partial I}{\partial t} \\ \frac{\partial I}{\partial x}\frac{\partial I}{\partial t} & \frac{\partial I}{\partial y}\frac{\partial I}{\partial t} & \frac{\partial I}{\partial t}^2 \end{bmatrix}.$$

Definition 2.3.2. (Spectral Direction Stability) Considering a vector $\vec{u}^T = [a, b, c]$ and a tensor $(\mathbf{T}) = \vec{u} \cdot \vec{u}^T$, the eigenvalues of $(\mathbf{T})$ are:

$$\begin{aligned} \beta_1^{(\mathbf{T})} &= a^2 + b^2 + c^2, \\ \beta_2^{(\mathbf{T})} &= 0, \\ \beta_3^{(\mathbf{T})} &= 0, \end{aligned}$$

and its respective eigenvectors are:

$$\vec{V}_1^T = \begin{bmatrix} a \\ b \\ c \end{bmatrix}, \vec{V}_2^T = \begin{bmatrix} b \\ -a \\ 0 \end{bmatrix}, \vec{V}_3^T = \begin{bmatrix} ac \\ bc \\ -(a^2+b^2) \end{bmatrix},$$

forming an orthogonal basis.

The tensors $(\mathbf{T_i}), i = 1, 2, 3$ are defined as the product $\vec{V}_i \cdot \vec{V}_i^T$. $(\mathbf{T_1})$ is the original tensor, so its eigenvectors are $V_1^{\mathbf{T_1}} = U, V_2^{\mathbf{T_1}} = V_2, V_3^{\mathbf{T_1}} = V_3$. For tensor $(\mathbf{T_3})$, we have

$(\mathbf{T_3}) = \vec{V}_3 \cdot \vec{V}_3^T$. The eigenvalues of $(\mathbf{T_3})$ are:

$$\beta_1^{(\mathbf{T_3})} = (a^2 + b^2)(a^2 + b^2 + c^2),$$
$$\beta_2^{(\mathbf{T_3})} = 0,$$
$$\beta_3^{(\mathbf{T_3})} = 0,$$

and the eigenvectors are:

$$\vec{V}_1^{(\mathbf{T_3})} = \begin{bmatrix} ac \\ bc \\ -(a^2 + b^2) \end{bmatrix}, \vec{V}_2^{(\mathbf{T_3})} = \begin{bmatrix} b \\ -a \\ 0 \end{bmatrix}, \vec{V}_3^{(\mathbf{T_3})} = \begin{bmatrix} a \\ b \\ c \end{bmatrix}.$$

This way, we have:

$$\vec{V}_1^{(\mathbf{T_1})} = \vec{V}_3^{(\mathbf{T_3})}, \vec{V}_2^{(\mathbf{T_1})} = \vec{V}_2^{(\mathbf{T_3})}, \vec{V}_3^{(\mathbf{T_1})} = \vec{V}_1^{(\mathbf{T_3})}. \quad (2.8)$$

This property is called *spectral direction stability of* $(\mathbf{T})$ *tensor.*

For the structure tensor of a pixel $(\mathbf{S})$ defined above, the spectral elements of are the eigenvalues:

$$\beta_1^{(\mathbf{S})} = \frac{\partial I}{\partial x}^2 + \frac{\partial I}{\partial y}^2 + \frac{\partial I}{\partial t}^2,$$
$$\beta_2^{(\mathbf{S})} = 0,$$
$$\beta_3^{(\mathbf{S})} = 0.$$

The eigenvector associated to $\beta_1^{(\mathbf{S})}$ is the gradient vector $\vec{V}_1^{(\mathbf{S})} = \nabla I$. The subspace generated by the two other eigenvectors is orthogonal to ∇I, so any vector belonging to the kernel of $(\mathbf{S})$ is a solution of the main optical flow constraint (Equation 2.4). To form a direct orthogonal basis, $\vec{V}_2^{\mathbf{S})}$ and $\vec{V}_3^{\mathbf{S})}$ can be:

$$\vec{V}_1^S = \begin{bmatrix} \frac{\partial I}{\partial x} \\ \frac{\partial I}{\partial y} \\ \frac{\partial I}{\partial t} \end{bmatrix}, \vec{V}_2^S = \begin{bmatrix} \frac{\partial I}{\partial y} \\ -\frac{\partial I}{\partial x} \\ 0 \end{bmatrix}, \vec{V}_3^S = \begin{bmatrix} \frac{\partial I}{\partial x} \cdot \frac{\partial I}{\partial t} \\ \frac{\partial I}{\partial y} \cdot \frac{\partial I}{\partial t} \\ -(\frac{\partial I}{\partial x}^2 + \frac{\partial I}{\partial t}^2) \end{bmatrix}.$$

Extending this approach to a three-bands image, consider that the gradient vector $\vec{g} = [\nabla I_1, \nabla I_2, \nabla I_3]$. The multidimensional structure tensor $(\mathbf{G})$ in this case is obtained by:

$$(\mathbf{G}) = \sum_{j=1}^{3} \nabla I_j \cdot \nabla I_j^T, (\mathbf{G}) = \sum_{j=1}^{3} S_j,$$

where S_j is the structure tensor of the j-th channel. $(\mathbf{G})$ have three real eigenvalues distinct and positive. Considering $\beta_1^{(\mathbf{G})}$ as the dominant eigenvalue and $V_1^{(\mathbf{G})}$ as the associated eigenvector, $V_1^{(\mathbf{G})}$ is the direction of maximal variation, Augereau considers the direction $V_1^{(\mathbf{G})}$ as the multiband gradient:

$$\nabla I = \vec{V}_1^{(\mathbf{G})}.$$

The optical flow vector $\vec{v}$ should then be in the orthogonal subspace, defined by $\vec{V}_2^{(\mathbf{G})}$ and $\vec{V}_3^{(\mathbf{G})}$. There is no direct indication of how to interpret the two last spectral directions; it is not possible to state, for example, that flow will be linked to the direction $\vec{V}_3^{(\mathbf{G})}$ associated to the smallest eigenvalue, because each band structure tensor $(\mathbf{S_j})$ has two null eigenvalues. This problem is solved by applying the Equation 2.8 of spectral directions stability. Flow tensor $(\mathbf{F_j})$ is defined as

$$(\mathbf{F_j}) = V_3^{(\mathbf{S_j})} \cdot V_3^{(\mathbf{S_j})T}, \tag{2.9}$$

where $V_3^{(S_j)} = \vec{v}_j$ is the optical flow from the structure tensor of the j channel. Its eigenvalues are:

$$\beta_1^{(\mathbf{T_3})} = (\frac{\partial I}{\partial x}^2 + \frac{\partial I}{\partial y}^2)(\frac{\partial I}{\partial x}^2 + \frac{\partial I}{\partial y}^2 + \frac{\partial I}{\partial t}^2),$$

$$\beta_2^{(\mathbf{T_3})} = \beta_3^{(\mathbf{T_3})} = 0,$$

with eigenvectors:

$$\vec{V}_1^{(\mathbf{F_j})} = \begin{bmatrix} -(\frac{\partial I}{\partial x}^2 + \frac{\partial I}{\partial t}^2) \\ \frac{\partial I}{\partial y} \cdot \frac{\partial I}{\partial t} \\ \frac{\partial I}{\partial x} \cdot \frac{\partial I}{\partial t} \end{bmatrix} = \vec{v}_j, \vec{V}_2^{(\mathbf{F_j})} = \begin{bmatrix} \frac{\partial I}{\partial y} \\ -\frac{\partial I}{\partial x} \\ 0 \end{bmatrix} = \vec{V}_2^{(\mathbf{S_j})}, \vec{V}_3^{(\mathbf{F_j})} = \begin{bmatrix} \frac{\partial I}{\partial x} \\ \frac{\partial I}{\partial y} \\ \frac{\partial I}{\partial t} \end{bmatrix} = \nabla I_j.$$

Having computed the flow tensors for each band, global flow tensor is build as:

$$(\mathbf{F}) = \sum_{j=1}^{3} (\mathbf{F_j}) = \sum_{j=1}^{3} \vec{v}_j \cdot \vec{v}_j^{(\mathbf{T})}. \tag{2.10}$$

The color optical flow $\vec{v}$ is defined in terms of the flow tensor as $V_1^{(\mathbf{F})}$, which is the direction given by the dominant eigenvalue. The computation of $\vec{v}$ is then possible by obtaining the roots of the characteristic polynomial of tensor $(\mathbf{F})$ and solving a linear system.

2.3.4 Revision of more recent works

Baker et al [5] addresses and evaluates a whole new generation of algorithms of optical flow, explaining some of the problem detected on traditional approaches and how those new methods contour them.

One of the problems detected on Horn's approach was the use of a L_2-norm, which implies the assumption of flow smoothness, which does not happen in practice. Black and Anandan [10] presented an algorithm capable of using an arbitrary penalty function. Some new differential methods [11, 34] used a L_1-norm as penalty function, changing the effect of the error penalty on discontinuities.

Another recent variant of research on optical flow is to use different pixel features, instead of using only intensity gradient. The work of Lui et al [21] uses SIFT-features to determine optical flow. Another possibility of optimization is to try to model illumination and blur, as made by the method of Seitz and Baker [29].

Some methods use continuous optimization techniques, such as gradient descent techniques [17, 18] or variational approaches [30, 35, 37] to solve optical flow. Gradient descent is a traditional method for nonlinear system resolution, based on local minimization using the gradient vector. Variational approaches are based on Euler-Lagrange minimization equations.

Another problem addressed is the use of multiband color images. Aside the work of Augereau et al [4], Zimmer et al [37] explores different ways of treating colored images, such as the use of HSV color space. Some other works related to multiband color images are Andrews [3], Golland and Bruckstein [13].

Some works are based on generating flow multiple times with a number of different parameters, and choosing for each pixel the best of the set of possible candidates. Lempitsky et al [18] uses this kind of approach.

It is also common to see methods based on “coarse-to-fine” heuristics. The first technique to use this kind of approach was [2]. This approach creates a “laplacian pyramid” with series of images from the input image with decreasing resolution. Optical flow is calculated on lower resolutions and its results are passed up in the pyramid as an initial guess of the next level. A recent approach based on the use of laplacian pyramids is the work of Xu et al [36], which presents a scale-invariant approach for optical flow.

The approaches of Li [19] and Sun et al [30] solve optical flow by generating a Markov random field model capable to learn optical flow pattern by training with ground-truth images. These methods have proven to be as precise as traditional methods to determine optical flow.

Also, some approaches work on method trying to improve performance. Parallel versions of optical flow were proposed in the work of Rannacher [28] anad more recently in Tao et al [31].

3 Computational Model

This chapter presents the computational model, i. e., details for implementation of the three differential methods described in Chapter 2.

3.1 Horn and Schunck

The computation of Horn and Schunck method is made by minimizing Equation 2.5, which corresponds to a weighted sum of the optical flow's main constraint and a smoothness constraint.

By using variational calculus and a digital estimation of the Laplacian, Horn and Schunck described the optical flow field by a large linear system with two equations for each pixel:

$$(\alpha^2 + \frac{\partial I}{\partial x}^2 + \frac{\partial I}{\partial y}^2)(u - \bar{u}) = -\frac{\partial I}{\partial x} \cdot (\frac{\partial I}{\partial x} \cdot \bar{u} + \frac{\partial I}{\partial y} \cdot \bar{v} + \frac{\partial I}{\partial t}),$$
$$(\alpha^2 + \frac{\partial I}{\partial x}^2 + \frac{\partial I}{\partial y}^2)(v - \bar{v}) = -\frac{\partial I}{\partial y} \cdot (\frac{\partial I}{\partial x} \cdot \bar{u} + \frac{\partial I}{\partial y} \cdot \bar{v} + \frac{\partial I}{\partial t}),$$

where $\bar{u}$ and $\bar{v}$ are the averages of the component of the flow vector in a small neighborhood around the current pixel (x, y). The value of α is used to prevent wrong adjustments of the flow occasioned by the noise derivative estimates. This parameter must be proportional to the expected noise in the estimation of the derivatives.

The resulting linear system is sparse and very large, since there are two equations per pixel. Therefore, direct methods such as Gauss-Jordan elimination are computationally expensive to this problem, and iterative methods such as Gauss-Seidel are a better choice. The iterative step of the optical flow estimative is:

$$\begin{aligned} u^{n+1} &= \bar{u}^n - \frac{\frac{\partial I}{\partial x} \cdot (\frac{\partial I}{\partial x} \cdot \bar{u}^n + \frac{\partial I}{\partial y} \cdot \bar{v}^n + \frac{\partial I}{\partial t})}{\alpha^2 + \frac{\partial I}{\partial x}^2 + \frac{\partial I}{\partial y}^2}, \\ v^{n+1} &= \bar{v}^n - \frac{\frac{\partial I}{\partial y} \cdot (\frac{\partial I}{\partial x} \cdot \bar{u}^n + \frac{\partial I}{\partial y} \cdot \bar{v}^n + \frac{\partial I}{\partial t})}{\alpha^2 + \frac{\partial I}{\partial x}^2 + \frac{\partial I}{\partial y}^2}. \end{aligned} \tag{3.1}$$

In homogeneous parts of the image, the estimation will be the average value of the neighboring velocity estimates. For constrained regions, the apparent velocity of the borders shall propagate itself through the region in a number of iterations. Therefore, the progress effects of a flow field during the iterative process can be associated to solution of heat diffusion equation for an uniform flat plate.

For instance, consider a single square object: the first estimative of optical flow will consider only the gradient property. Therefore, due to aperture problem, along the edges only the normal component is estimated. At the corner all components are estimated, and inside the square the optical flow vector is null, since gradient is zero. During the iterative process, the missing component of the borders will be filled by propagation from the corners, and then the flow shall diffuse through the inside of the square [26].

The original article from Horn and Schunck recommends setting the number of iterations larger than the number of cells on the largest region to be filled in.

For a sequence of more than two images, it is possible to set the flow from the previous time-step as initial value of the current time-step field, optimizing the estimative.

3.2 Lucas-Kanade

Lucas and Kanade [20] solves optical flow by assuming similarity in a small neighborhood around the pixel, which is described by Equation 2.7. Solution for this equation satisfies:

$$A^T \cdot W^2 \cdot A \cdot \vec{v} = A^T \cdot W^2 \cdot b,$$

where:

$$\begin{aligned} A &= [\nabla I(\vec{p}_1), \nabla I(\vec{p}_2), \cdots, \nabla I(\vec{p}_n)]^T, \\ W &= diag[W(x_1), W(x_2), \cdots, W(x_n)], \\ \vec{b} &= -[I_t(x_1), I_t(x_2), \cdots, I_t(x_n)]^T. \end{aligned}$$

The solution to the system is:

$$\vec{v} = [A^T \cdot W^2 \cdot A]^{-1} A^T \cdot W^2 \cdot \vec{b}. \tag{3.2}$$

The system is overdetermined, since the number of equations is proportional to the number of neighbours. It can be solved in closed form when $A^T \cdot W^2 \cdot A$ is nonsingular, since it is a 2x2 matrix:

$$A^T \cdot W^2 \cdot A = \begin{bmatrix} \sum_{p\in\Omega} W^2(x) \frac{\partial I(\vec{p})}{\partial x}^2 & \sum_{p\in\Omega} W^2(x) \frac{\partial I(\vec{p})}{\partial x} \frac{\partial I(\vec{p})}{\partial y}, \\ \sum_{p\in\Omega} W^2(x) \frac{\partial I(\vec{p})}{\partial y} \frac{\partial I(\vec{p})}{\partial x} & \sum_{p\in\Omega} W^2(x) \frac{\partial I(\vec{p})}{\partial y}^2. \end{bmatrix}$$

This eases the process of obtaining the inverse matrix. For a 2x2 matrix

$$A = \begin{bmatrix} a & b \\ c & d \end{bmatrix},$$

it is possible to compute inverse matrix by using the following property:

$$A^{-1} = \frac{1}{detA} * adj(A),$$

where $adj(A)$ is the adjugate matrix of A, which in 2x2 case is:

$$adj(A) = \begin{bmatrix} d & -b \\ -c & a \end{bmatrix},$$

and $det(A) = a \cdot d - b \cdot c$.

With the inverse matrix computation, Equation 3.2 can be directly solved by a matrix multiplication process.

3.3 Augereau

The optical flow vector on Augereau's approach is defined as the vector associated to the first eigenvalue of the global flow tensor F. As demonstrated in Section 2.3.3, the global flow tensor is the sum of each band's tensor. To obtain flow tensor for each band is to build the structure tensor of each point, to find the three eigenvalues and to use Equation 2.9.

A possible simplification on the process is obtained by the use of the quadractic form property:

Definition 3.3.1. (Vector projection and quadratic form)

Considering a vector $\vec{u_j}^T = [a_j, b_j, c_j]$ and the tensor $(\mathbf{Q_j}) = \vec{u_j} \cdot \vec{u_j}^T$. Now consider a matrix q in which each row j is a vector u_j. We associate tensor $(\mathbf{Q}) = q \cdot q^T$. Tensor $(\mathbf{Q})$ verifies:

$$(\mathbf{Q}) = \sum_{j=1}^{n} \vec{u}_j \cdot \vec{u}_j^T, (\mathbf{Q}) = \sum_{j=1}^{n} (\mathbf{Q_j}),$$

where $(\mathbf{Q_j})$ is the tensor associated to the $\vec{u}_j$ vector.

Now, consider an arbitrary vector $\vec{v}$. Evaluating product $(\mathbf{Q}) \cdot \vec{v}$, it is:

$$(\mathbf{Q}) \cdot \vec{v} = \sum_{j=1}^{n} (\vec{u_j}^T \cdot \vec{v}) \cdot \vec{u_j},$$

which is the projection of a vector V relative to the matrix element q. In a similar way:

$$\vec{v}^T (\mathbf{Q}) \cdot \vec{v} = \sum_{j=1}^{n} (\vec{u_j}^T \cdot \vec{v}) \cdot \vec{v}^T \cdot \vec{u_j}.$$

$$\vec{v}^T (\mathbf{Q}) \cdot \vec{v} = \sum_{j=1}^{n} (\vec{u_j}^T \cdot \vec{v})^2. \tag{3.3}$$

This is the quadratic form applied to a vector $\vec{v}$ and defined by the set of vectors $[\vec{u}_1, \cdots, \vec{u}_n]$.

Modifying Equation 2.10 by applying this property, it is possible to construct the quadratic form of a matrix defined by vectors $\vec{v}_j$ applied to the global flow vector $\vec{v}$:

$$\vec{v}^T (\mathbf{F}) \vec{v} = \sum_{j=1}^{3} (\vec{v}_j \cdot \vec{v})^2.$$

Since $\vec{v}$ is a spectral element of $(\mathbf{F})$:

$$(\mathbf{F}) \cdot \vec{v} = \beta_1^{(\mathbf{F})} \cdot \vec{v},$$

therefore optical flow can be calculated iteratively, by making:

$$\begin{array}{rl} \beta_1^{(\mathbf{F}),k} & = \sum_{j=1}^{3} \left(\frac{\vec{v}_j^T \cdot \vec{v}^{k-1}}{||\vec{v}^{k-1}||} \right)^2 \\ v^k & = \frac{1}{\beta_1^{(\mathbf{F}),k-1}} \sum_{j=1}^{3} \left(\vec{v}_j^T \cdot \vec{v}^{k-1} \right) \vec{v}_j \end{array} \tag{3.4}$$

However, this is an alternative to computation of the characteristic polynomial of the tensor and resolution of a linear system.

4 Performance Evaluation

4.1 Error evaluation of Optical Flow

Barron and Beauchemin [8]'s benchmark to Optical Flow was one of the first benchmarks published in computer vision. This work proposed an absolute evaluation metric for optical flow techniques. Recently, several new approaches to optical flow were developed, and Barron's benchmark cryteria became insufficient to evaluate new features of those approaches.

Baker et al [6] proposed a new benchmark for optical flow evaluation. Along with the publication of the new benchmark, the Middlebury University Computer Vision's research team disponibilized on link `http://vision.middlebury.edu/flow/` [1] a dataset of ground-truth images, which were used to evaluate results on new methods. When a new optical flow method is developed, the author has now the option of evaluating his method on the benchmark, so that its precision and execution time can be compared to the other methods previously submitted. Even if the method wasn't yet published on a conference, it can be evaluated and its results are posted as a blind submission.

The proposal was effective and in 2011, Baker et al [5] published a survey with results of optical flow recent methods evaluation. At current date, 91 optical flow methods have been evaluated by Middlebury's benchmark.

The set of cryteria evaluated on this benchmark are:

Definition 4.1.1. Angular Error (AE) : This is the a popular measure of performance, proposed by Fleet and Jepsen [12] and used for evaluation of classic methods on Barron and Beauchemin [8]'s survey.

The error between two vectors $[u_0, v_0]$ and $[u_1, v_1]$ is the angle in 3D space between $[u_0, v_0, 1.0]$ and $[u_1, v_1, 1.0]$. Usually it is computed by normalizing the vectors, taking dot

[1] Middlebury benchmark for optical flow: http://vision.middlebury.edu/flow/. Access date: 22/08/2013.

product and then taking the inverse cosine of dot product:

$$e_{AE}(\vec{u}_0, \vec{u}_1) = cos^{-1} \frac{(\vec{u}_0 \cdot \vec{u}_1)}{||\vec{u}_1|| \cdot ||\vec{u}_0||}.$$

This measure penalizes error in large flows more than error in small flows.

Definition 4.1.2. Flow Endpoint (EP): This is the error defined by the L_2 norm of the difference between flow vectors $[u_0, v_0]$ and $[u_1, v_1]$:

$$e_{EP}(\vec{u}_0, \vec{u}_1) = \sqrt{(u_0 - u_1)^2 + (v_0 - v_1)^2}.$$

Unlike the angular error measurement, it does not penalize error resulting from large displacements more than small displacements.

For evaluation of methods previously described on Chapters Two and Three, this work will follow Baker et al [6]'s benchmark cryteria. But the ground-truth data refering to Middlebury's evaluation datasets is not directly available, and a process of submission of details from the publication is necessary to obtain evaluation ground-truth values. The evaluation of results is manual and a results table is provided to the author of the method. Since this work does not propose new approaches to optical flow, there was no necessity of a submission and we decided to use the public datasets provided on Middlebury's page, for which ground-truth results are available. All tests were executed on a computer with the following configurations: Intel Core 2 Quad, 2.83GHz, 4GB memory, Windows 7 64 bits.

4.2 Ground-Truth Flow

Baker's benchmark proposed a new representation for optical flow, due to high density of flow obtained in some methods. The flow is normalized and visualized as an HSV image, where hue indicates flow direction, saturation indicates flow intensity and value is 1. Figures 4.1, 4.2, 4.3 and 4.4 show examples of correlation between the color image and the vector field.

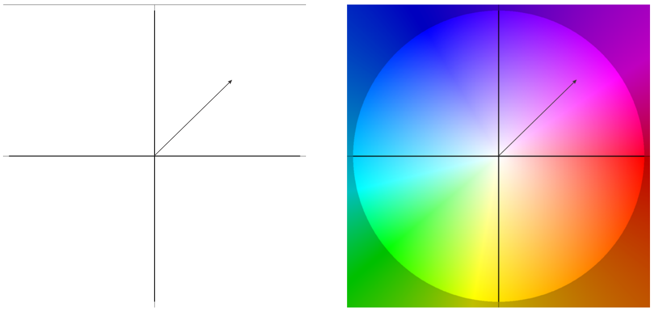

Figure 4.1: Example of mapping flow vector into RGB space.

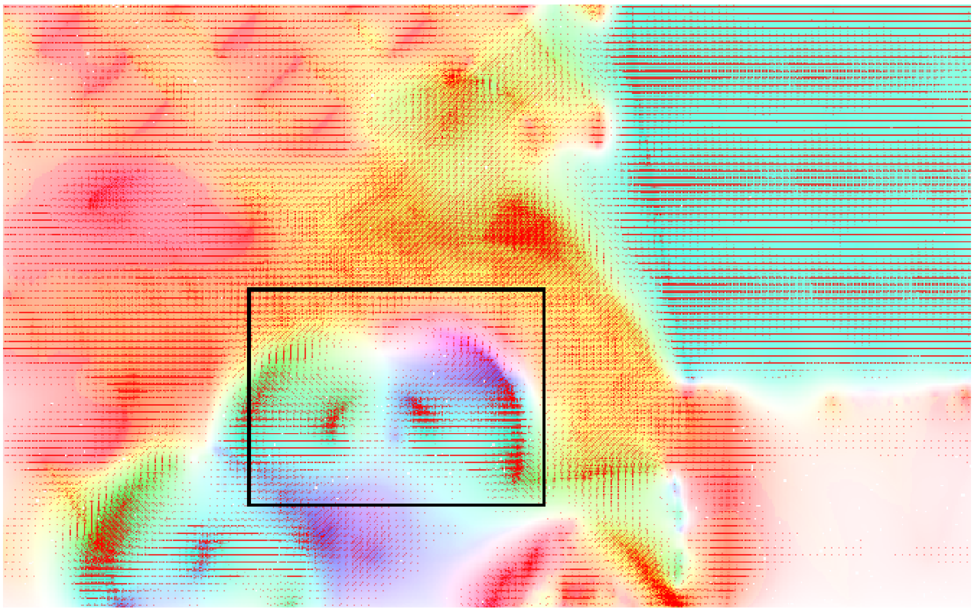

Figure 4.2: Example of correspondence between a color flow image and a vector flow field.

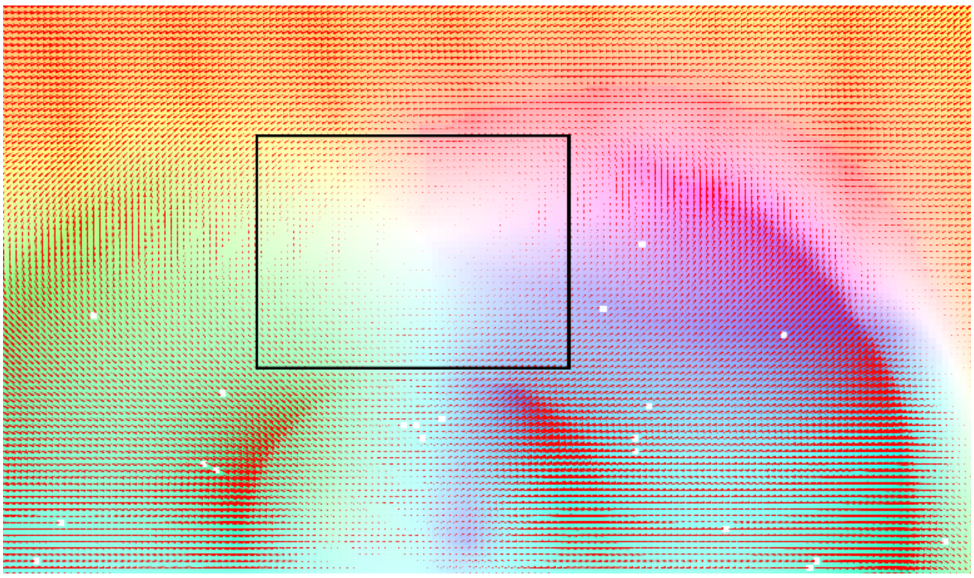

Figure 4.3: Example of correspondence between a color flow image and a vector flow field.

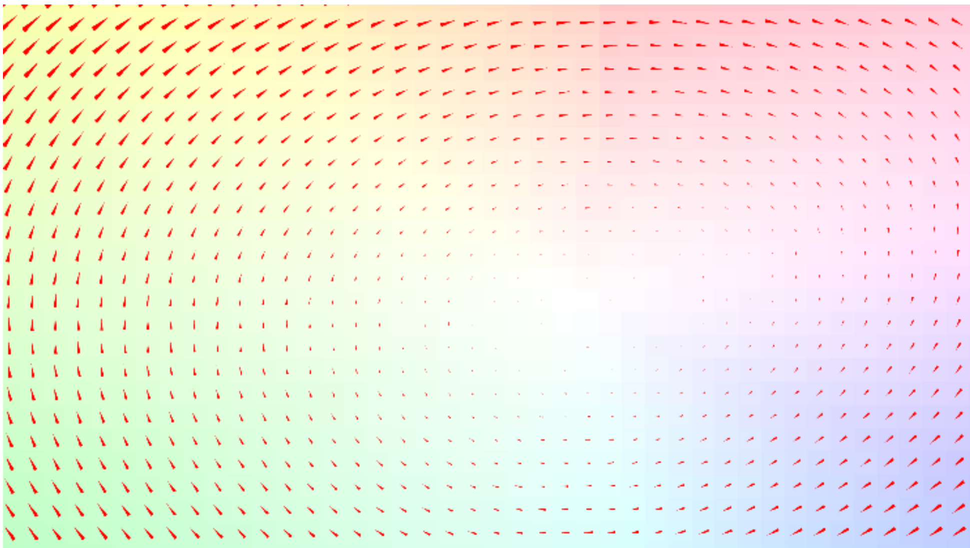

Figure 4.4: Example of correspondence between a color flow image and a vector flow field.

4.3 Comparison Results

As mentioned above, evaluation cryteria used on this work were average and standard deviation values for the angular error and flow endpoint for each image. Density of flow field and average time ellapsed were also measured. The methods were evaluated for the ground-truth image sequences available on Figures 4.5, 4.6, 4.7, 4.8 and 4.9.

- **Hydrangea**:

Figure 4.5: Both images and ground truth flow for **Hydrangea** sequence.

- **Rubber Whale**:

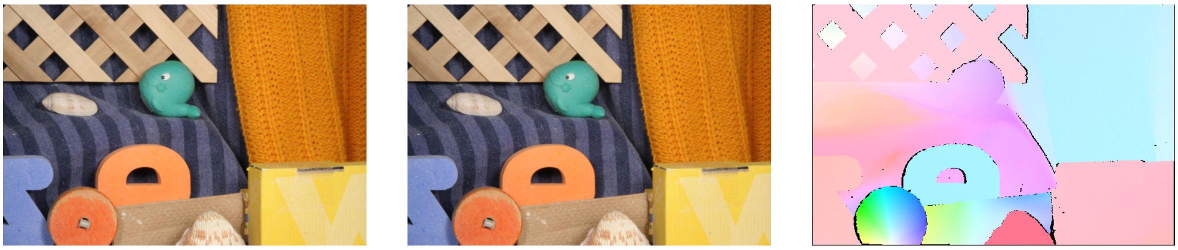

Figure 4.6: Both images and ground truth flow for **Rubber Whale** sequence.

- **Urban2**:

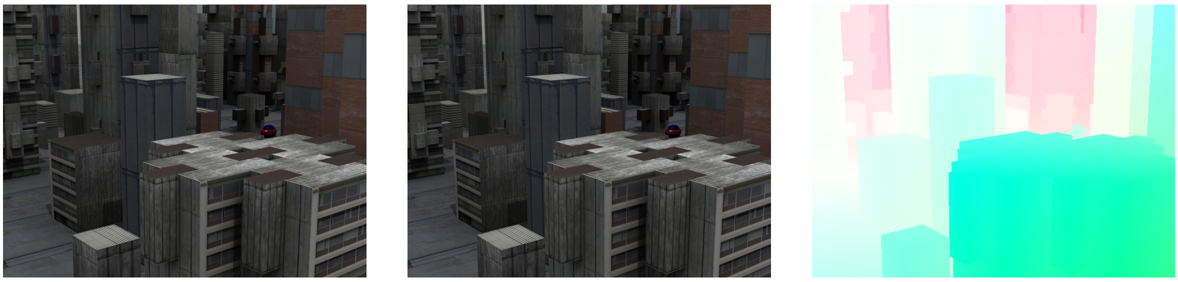

Figure 4.7: Both images and ground truth flow for **Urban2** sequence.

- **Dimetrodon**:

Figure 4.8: Both images and ground truth flow for **Dimetrodon** sequence.

- **Grove2**:

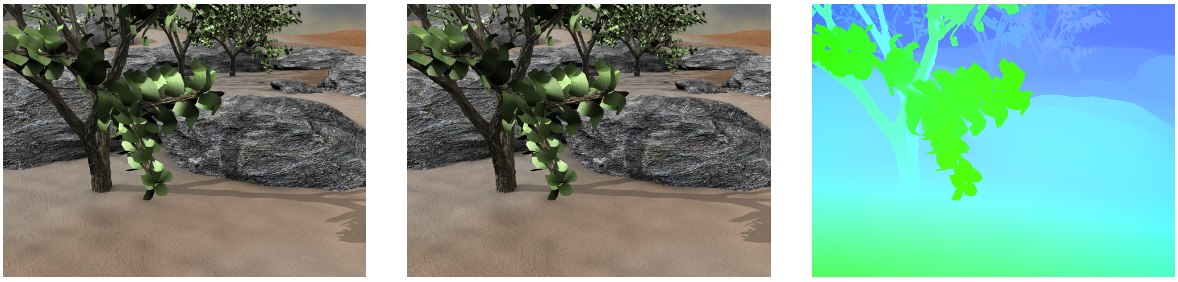

Figure 4.9: Both images and ground truth flow for **Grove2** sequence.

For Augereau's method, the flow was evaluated and the error measured to color images, and the methods of Lucas and Kanade and Horn and Schunck considered grayscale images.

On the evaluation tables, AVG AE and AVG EP are average values for the angular error (in degrees) and the flow endpoint (in pixels) on each pixel. SD AE (degrees) and SD EP (pixels) are standard deviation for angular error and flow endpoint. DENSITY (percentual) is the percentage of flow vectors considered "valid", and TIME (in seconds) is total time of the method's execution.

For density measurement, we considered that displacements larger than 20 pixels per frame were mismatching assignments from the method. Therefore, only pixels with flow norm smaller than 20 pixels per frame were considered on error computation. Density measured is the percentage of pixels on the image with valid flow measurements.

4.3.1 Horn and Schunck

On Horn and Schunck implementation, the algorithm was executed considering different α values. The parameter α is the weight of smoothness term relative to the gradient constraint term.

Considering $\alpha \in [0.1, 0.3, 0.5, 0.8, 1, 3]$, the error values were evaluated for 1000 iterations on each image. The results are presented on Table 4.1, and Figures 4.10, 4.11, 4.12, 4.13 and 4.14 presents the best estimative obtained for each image.

	α	AVG AE	AVG EP	SD AE	SD EP	DENSITY	TIME
Hydrangea	1	31,271	3,063	38,895	1,283	93,119	39,72
RubberWhale	5	35,106	0,864	43,125	0,694	98,010	39,36
Urban2	1	68,922	8,162	44,386	8,206	98,910	53,21
Dimetrodon	1	50,992	1,785	30,034	0,734	95,018	38,82
Grove2	5	61,633	2,796	41,195	0,926	99,034	53,35

Table 4.1: Horn and Schunck - Results with lower flow endpoint for each example.

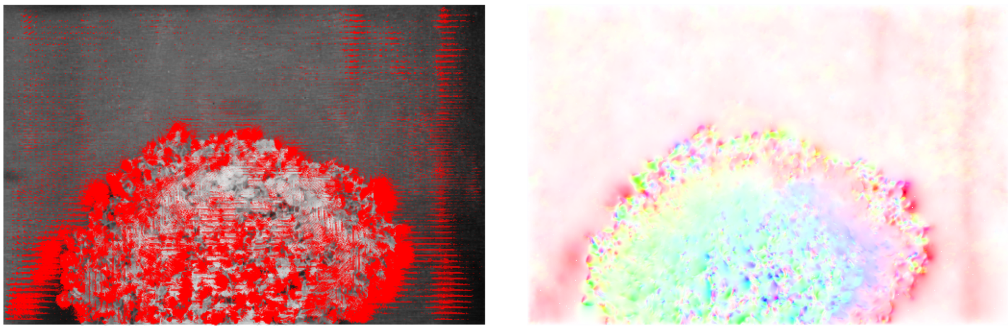

Figure 4.10: Optical flow field estimated by Horn and Schunck for Hydrangea example.

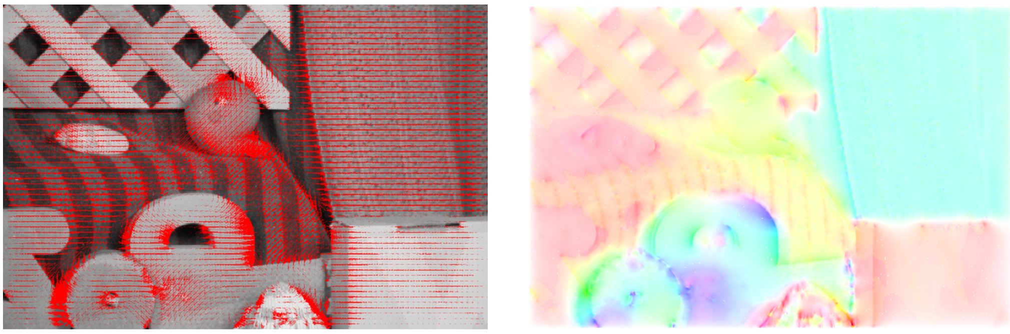

Figure 4.11: Optical flow field estimated by Horn and Schunck for Rubber Whale example.

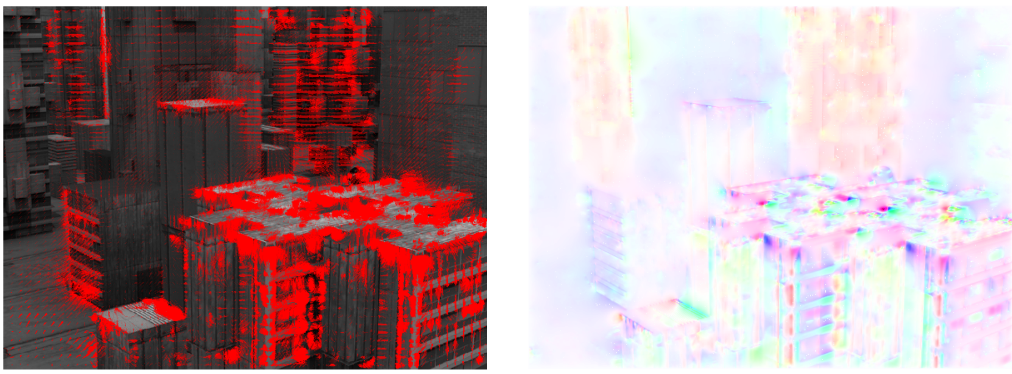

Figure 4.12: Optical flow field estimated by Horn and Schunck for Urban2 example.

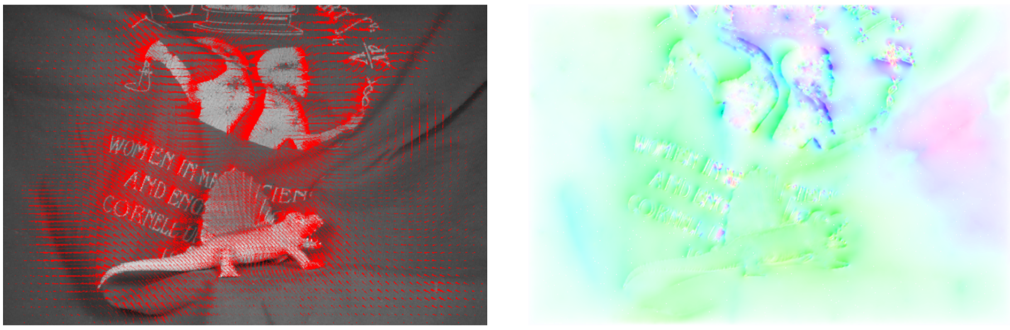

Figure 4.13: Optical flow field estimated by Horn and Schunck for Dimetrodon example.

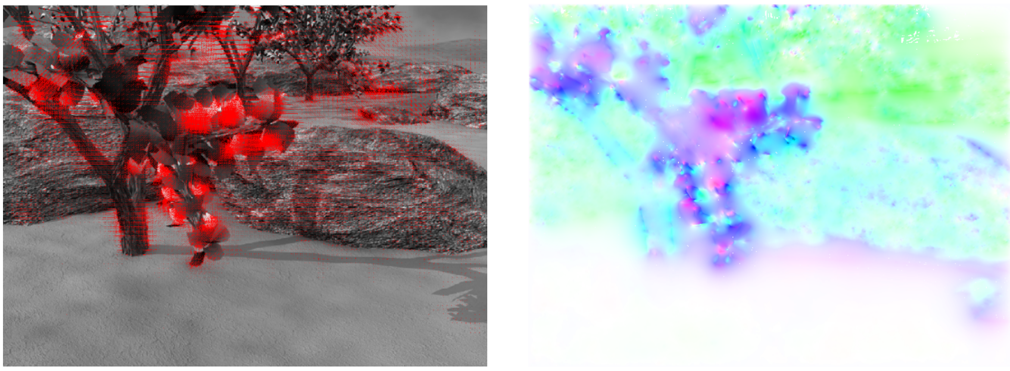

Figure 4.14: Optical flow field estimated by Horn and Schunck for Grove2 example.

It is also interesting to see the flow diffusion evolution through the iterations. For Grove2 Example, we plotted the vectorial field for 1, 10, 50, 100, 500 and 1000 iterations. The results are presented on Figures 4.15 and 4.16, on vectorial and color representation, respectively.

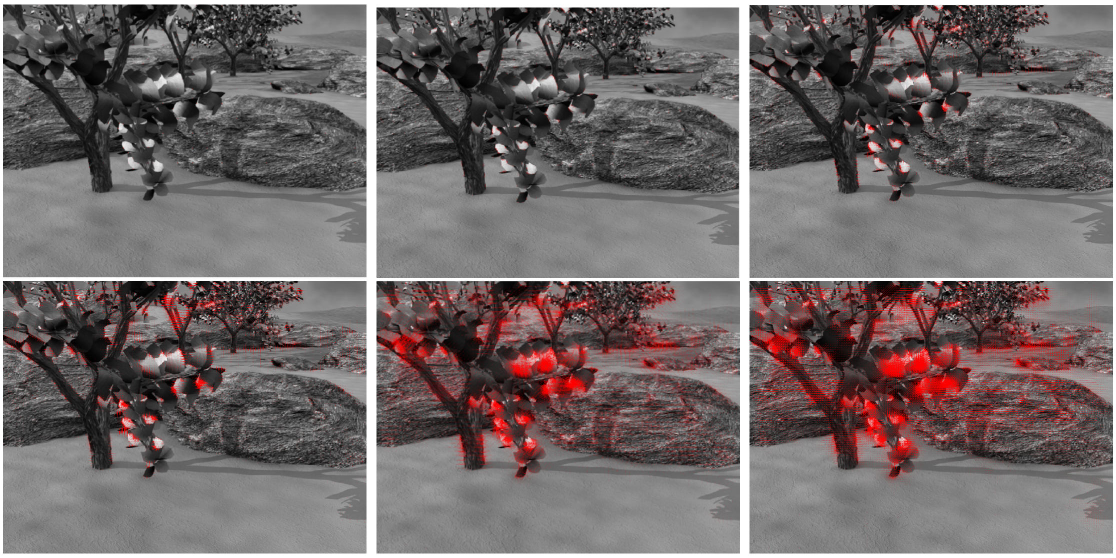

Figure 4.15: Flow evolution for Horn and Schunck Method, with 1, 10, 50, 100, 500 and 1000 iterations.

Figure 4.16: Color representation of flow evolution for Horn and Schunck Method, with 1, 10, 50, 100, 500 and 1000 iterations.

On the small region of Grove2 example presented on Figure 4.17, it is possible to see how the diffusion solves the aperture problem, making the flow diffuse through homogeneous regions:

The parameter α indicates velocity of diffusion. For small values of α, the weight of the gradient constraint is bigger than the smoothness constraint, as we can see in Equation 2.5. This indicates that diffusion process occasioned by smoothness constraint will occur slowly, and more iterations will be necessary for achieving a dense field.

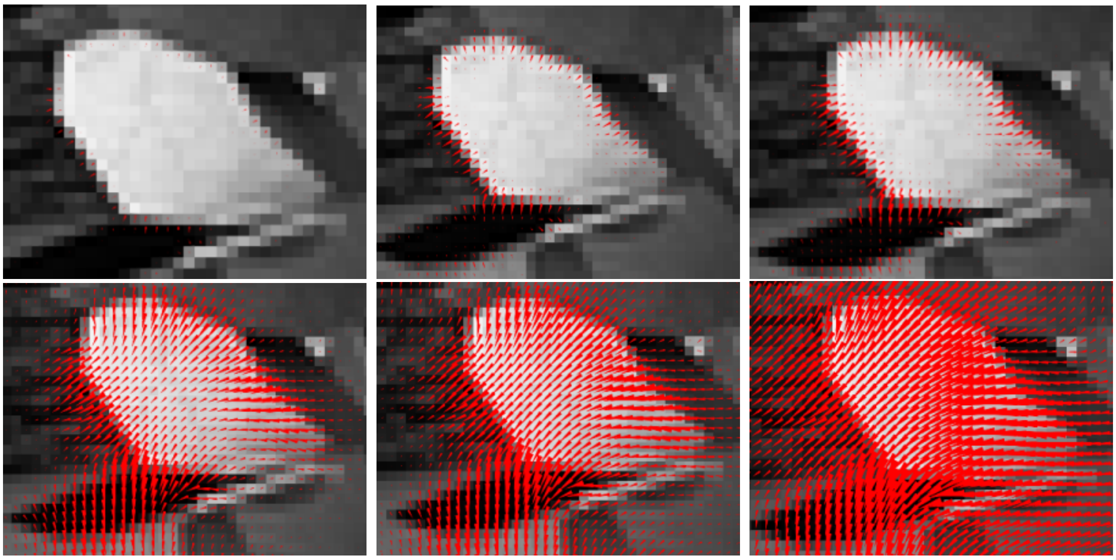

Figure 4.17: Flow evolution for a small region, with 1, 5, 10, 50, 100 and 500 iterations.

On the other hand, if $\alpha >> 1$, the algorithm is relying much more on the smoothness constraint then on the gradient constraint. This speeds convergence, but can occasionate loss of detail on the vector field obtained.

The original Horn and Schunck method [16] proposes using $\alpha = 100$. Barron and Beauchemin [8] obtained better results considering $\alpha = 0.5$. On this work, for most cases the better results are obtained considering $\alpha = 1$.

4.3.2 Lucas and Kanade

Lucas and Kanade method is dependent of two parameters: size of the gaussian filter W used and the standard deviation σ for the filter. The size of the mask influentiates the amount of neighbours taken in count for the computation. The standard deviation indicates the degree of smoothness of gaussian filter applied. For the optical flow estimation process, it can be seen as a measurement of precision on neighbor derivative estimatives.

This work used the same values considered by Barron and Beauchemin [8] for size of neighborhood and standard deviation. W is a 5x5 matrix, and $\sigma = 1.5$. Results obtained are on Table 4.2, and the estimatives obtained on each sequence for Lucas and Kanade method are on Figures 4.18, 4.19, 4.20, 4.21 and 4.22.

	AVG AE	AVG EP	SD AE	SD EP	DENSITY	TIME
Hydrangea	67,7421	3,70712	52,274	2,379	73,073	0,124
RubberWhale	39,468	1,34949	41,604	1,275	71,993	0,124
Urban2	79,0861	9,88212	49,681	9,123	52,9	0,166
Dimetrodon	66,7753	2,63076	39,82	1,966	27,997	0,122
Grove2	76,6741	3,45482	52,18	2,389	85,415	0,17

Table 4.2: Lucas and Kanade - Results with lower flow endpoint for each example.

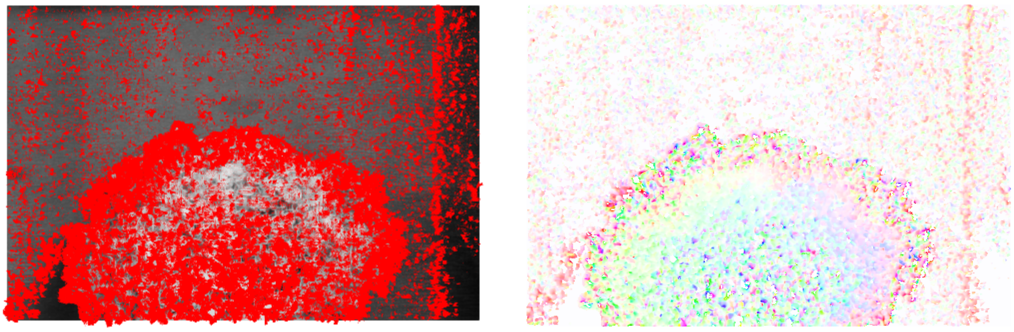

Figure 4.18: Optical flow field estimated by Lucas and Kanade for Hydrangea example.

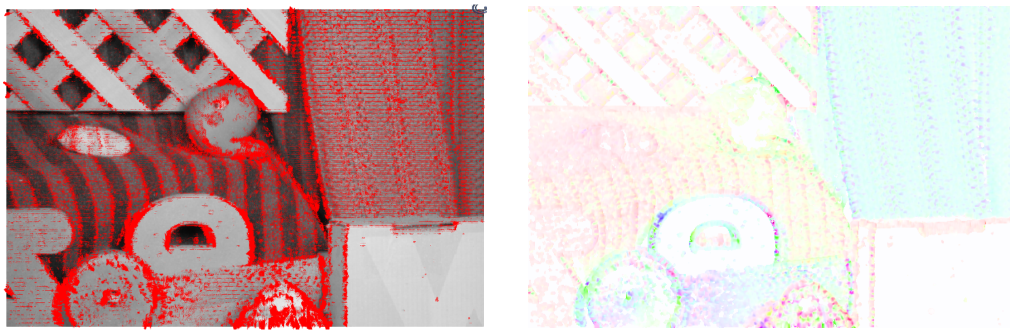

Figure 4.19: Optical flow field estimated by Lucas and Kanade for Rubber Whale example.

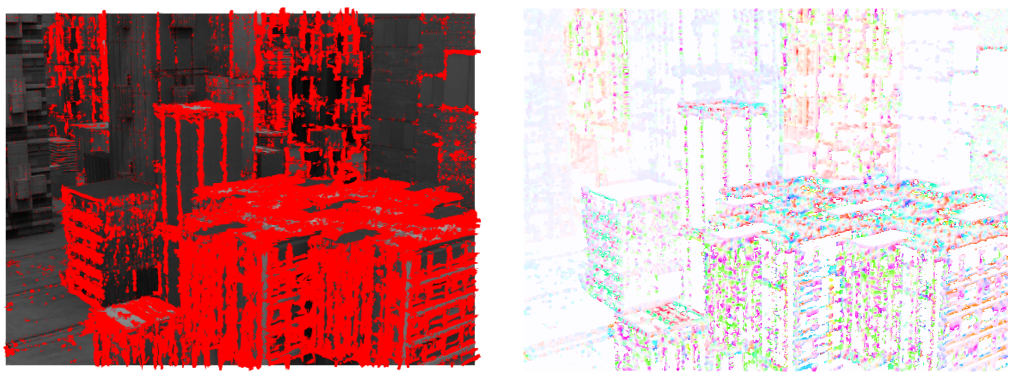

Figure 4.20: Optical flow field estimated by Lucas and Kanade for Urban2 example.

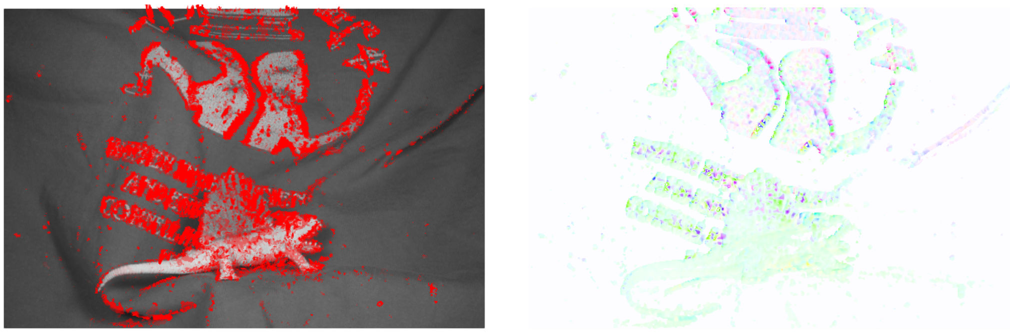

Figure 4.21: Optical flow field estimated by Lucas and Kanade for Dimetrodon example.

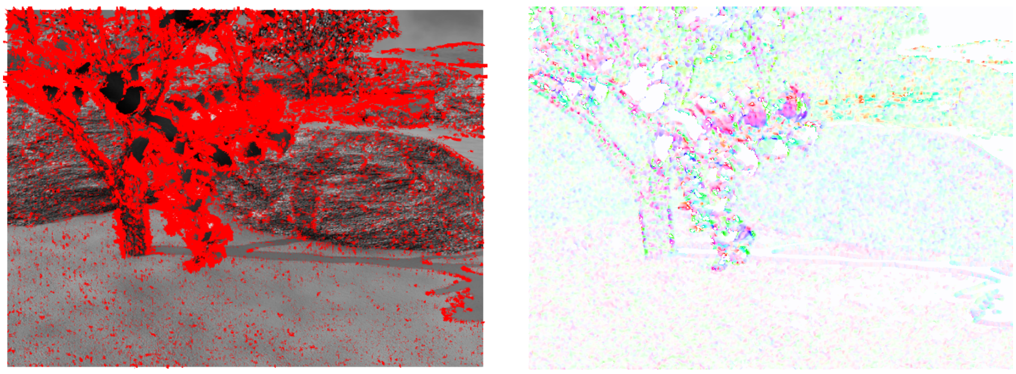

Figure 4.22: Optical flow field estimated by Lucas and Kanade for Grove2 example.

4.3.3 Augereau

The images evaluated for Augereau method are colored, differently from Horn and Schunck and Lucas and Kanade methods. Therefore, the results obtained may not reflect the real quality of Augereau method if compared to Horn and Schunck and Lucas and Kanade. For obtaining a fair comparative quality measurement, Augereau method should be evaluated with grayscale images.

Table 4.3 presents Augereau's results for each example. The estimatives obtained are presented on Figures 4.23, 4.24, 4.25, 4.26 and 4.27.

	AVG AE	**AVG EP**	**SD AE**	**SD EP**	**DENSITY**	**TIME**
Hydrangea	81,0153	4,67847	46,98844	2,987073	89,109	0,088
RubberWhale	61,26236	1,70489	44,49664	1,602105	89,242	0,084
Urban2	85,02931	9,79227	53,34374	8,87436	70,104	0,099
Dimetrodon	81,33943	2,902915	50,76337	2,29702	69,353	0,07
Grove2	88,61234	4,411229	48,20267	3,013752	87,137	0,111

Table 4.3: Augereau - Results for each example.

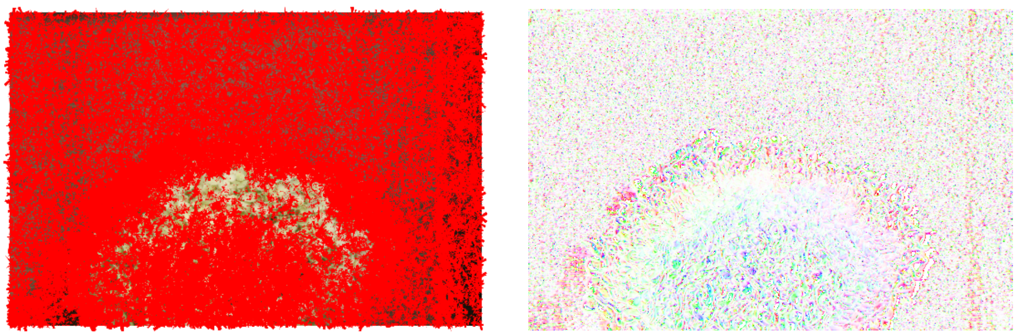

Figure 4.23: Optical flow field estimated by Augereau method for Hydrangea example.

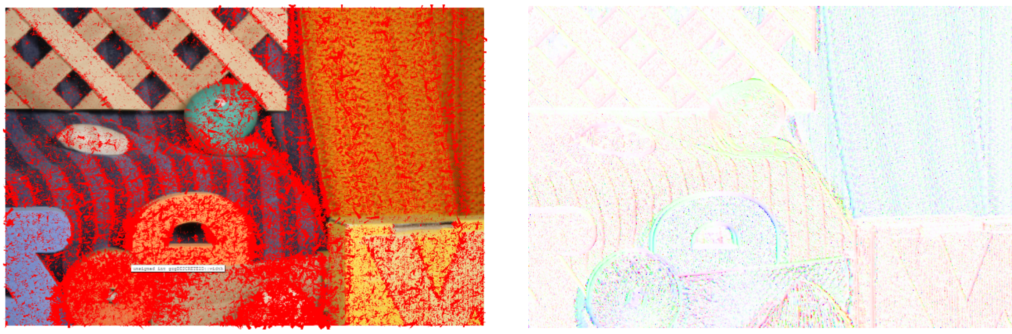

Figure 4.24: Optical flow field estimated by Augereau method for Rubber Whale example.

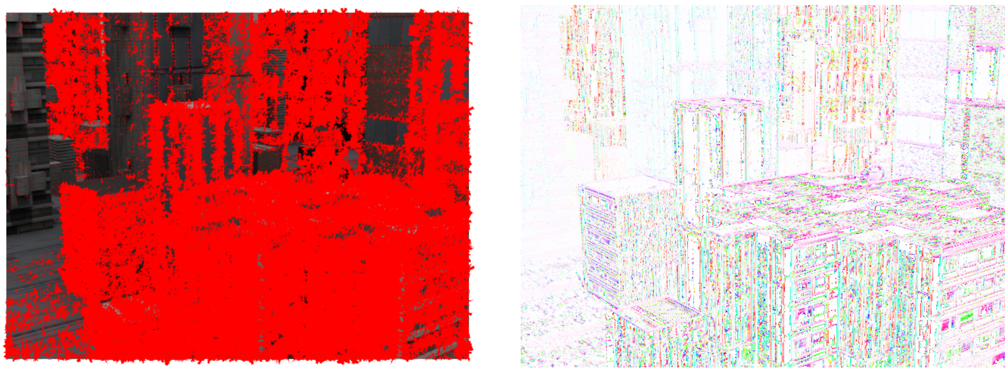

Figure 4.25: Optical flow field estimated by Augereau method for Urban2 example.

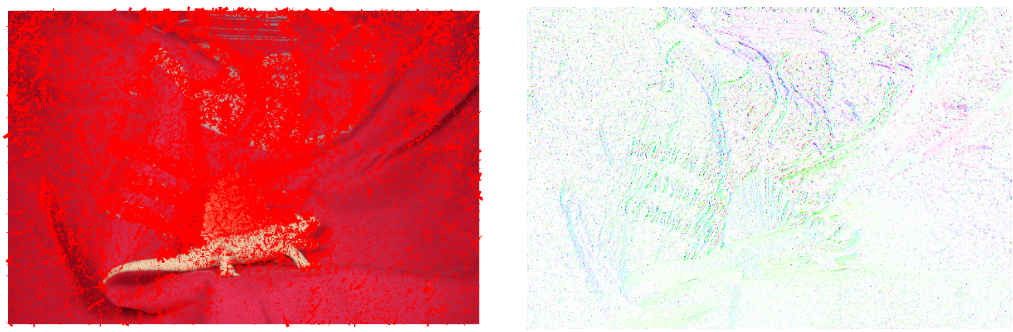

Figure 4.26: Optical flow field estimated by Augereau method for Dimetrodon example.

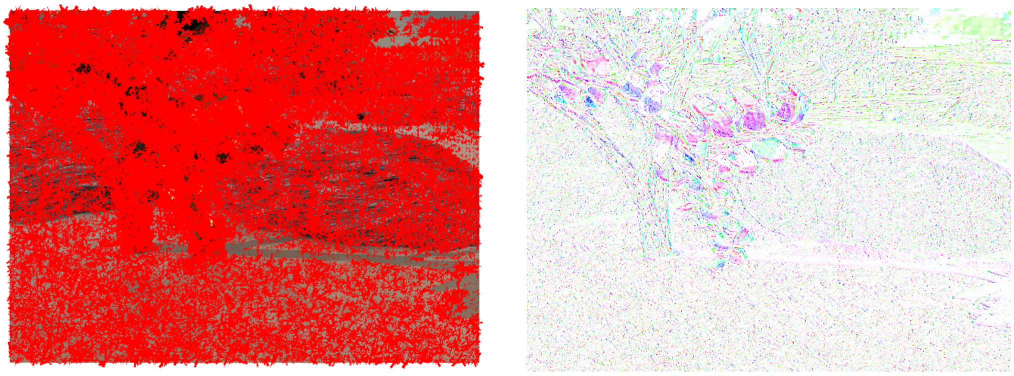

Figure 4.27: Optical flow field estimated by Augereau method for Grove2 example.

4.3.4 Analysis of Results

Table 4.4 shows a comparison of error results, density and time for each method.

		AVG AE	AVG EP	SD AE	SD EP	DENSITY	TIME
Hydrangea	**AUG**	81,015	4,678	46,988	2,987	89,109	0,088
	LK	67,742	3,707	52,274	2,379	73,073	0,124
	HS	31,271	3,063	38,895	1,283	93,119	39,72
RubberWhale	**AUG**	61,262	1,705	44,497	1,602	89,242	0,084
	LK	39,468	1,349	41,604	1,275	71,993	0,124
	HS	35,106	0,864	43,125	0,694	98,010	39,36
Urban2	**AUG**	85,029	9,792	53,344	8,874	70,104	0,099
	LK	79,086	9,882	49,681	9,123	52,9	0,166
	HS	68,922	8,162	44,386	8,206	98,910	53,21
Dimetrodon	**AUG**	81,339	2,903	50,763	2,297	69,353	0,07
	LK	66,775	2,631	39,820	1,966	27,997	0,122
	HS	50,992	1,785	30,034	0,734	95,018	38,82
Grove2	**AUG**	88,612	4,411	48,203	3,014	87,137	0,111
	LK	76,674	3,455	52,180	2,389	85,415	0,17
	HS	61,633	2,796	41,195	0,926	99,034	53,35

Table 4.4: Results with lower flow endpoint for each example and method.

As for the evaluation of results, it is possible to see that Horn and Schunck method presents more accurate results and more dense flow. In contrast, the precision enhancement of this method is directly proportional to the number of iterations executed, so the time spent is proportionally bigger then other methods.

Sequences analysed presents specific features: Hydrangea presents a rigid body angular movement. The flow on Grove2 is characterized by smooth rotation and translation. Urban2 presents a large displacement on part of the image, and the sequences RubberWhale and Dimetrodon presents multiple rigid objects moving.

Considering Angular Error, the best results on Augereau and Lucas-Kanade methods are on RubberWhale sequence, as Horn and Schunck works fine on Hydrangea. For Flow Endpoint, the best results for the three methods were on RubberWhale sequence. As for weak points, the error on Horn and Schunck's result on Urban2 sequence is very large, even considering 1000 iterations and nearly 40s execution time. On Augereau and Lucas Kanade, the worst Angular Error error was measured on Grove2 sequence.

Standard deviation was nearly constant on all sequences. For density, Horn and Schunck generates a dense flow in all cases. In opposition, the field generated on Lucas and Kanade method is sparse. Augereau is a reasonable mid-term in this cryteria.

In conclusion, for real-time dense optical flow computation, Augereau method is a good choice. For more precise computation, Horn and Schunck method is indicated.

5 Conclusion

This work begins by introducing basic flow dynamics concepts and Navier-Stokes equation, which are needed to understand the mathematical model of optical flow. Then, it was possible to define optical flow on an image, as well as three computation methods: Horn and Schunck, Augereau and Lucas and Kanade. Later, a brief summary of current research on area was presented. The computational model of the methods and possible optimizations on the process were described, such as the faster solution for Lucas and Kanade's linear system and the iterative scheme on Horn and Schunck algorithm. Then the methods were evaluated on Middlebury public dataset, and results show that iterative Horn and Schunck method obtained a more accurate result, despite its relatively high execution time.

It is always important to reaffirm that this work has no intention to compare methods with the current state-of-art of optical flow estimation methods at the moment. The intention here is mostly to give basic notions to the readers about the optical flow problem and classical solutions.

The top results on Middlebury evaluation dataset at the moment are from recent papers, or some methods that will yet be presented on conferences, whose results are posted on the site as a blind submission. This indicates that although modern methods achieve very high precision, optical flow estimative is still an open problem and yet a hot research topic on computer vision.

A - General solution for unidimensional movement

This is an extension of section 2.2.2. On that section, we evaluated displacement as a constant value h. It is possible to consider that displacement h is a value dependent of the total displacement x, i.e. $h(x) = g(x) - f(x)$. Hence, the problem is reduced to a linear non-homogeneous equation on the form:

$$\frac{dy}{dx} + P(x)y = Q(x),$$

for which solution is:

$$y = e^{-\int P(x)dx}[\int e^{\int P(x)dx} Q(x)dx + c_1].$$

Considering now the general equation for unidimensional movement:

$$\frac{dh}{dx} + h\frac{f'(x)}{f(x)} = 1 - \frac{g(x)}{f(x)}$$

Let $P(x) = \frac{f'(x)}{f(x)}, Q(x) = 1 - \frac{g(x)}{f(x)}$:

$$h(x) = e^{-\int \frac{f'(x)}{f(x)}dx}[\int e^{\int \frac{f'(x)}{f(x)}dx}(1 - \frac{g(x)}{f(x)})dx + c_1]$$

but $\int \frac{f'(x)}{f(x)}dx = \int \frac{df(x)}{dx}\frac{1}{f(x)}dx = \int \frac{df(x)}{f(x)} = lnf(x) + c_2$

$$h(x) = e^{-(lnf(x)+c_2)}[\int e^{(lnf(x)+c_3)}(1 - \tfrac{g(x)}{f(x)})dx + c_1]$$
$$h(x) = \tfrac{e^{lnf(x)^{(-1)}}}{e^{c_2}}[\int e^{c_3}e^{lnf(x)}(1 - \tfrac{g(x)}{f(x)})dx + c_1]$$
$$h(x) = \tfrac{1}{e^{c_2}}\tfrac{1}{f(x)}[\int e^{c_3}f(x)(1 - \tfrac{g(x)}{f(x)})dx + c_1]$$
$$h(x) = \tfrac{1}{e^{c_2}}\tfrac{1}{f(x)}[\int e^{c_3}[f(x) - g(x)]dx + c_1]$$
$$h(x) = \tfrac{c_1 + e^{c_3}[\int (f(x)-g(x))dx]}{e^{c_2}f(x)}$$

Bibliography

[1] Acheson, D. J. **Elementary fluid dynamics**. Oxford University Press, 1990.

[2] Bergen, J. R.; Anandan, P.; Hanna, K. J. ; Hingorani, R. **Hierarchical model-based motion estimation**. In: Computer Vision CCV92, p. 237–252. Springer, 1992.

[3] Andrews, R. J.; Lovell, B. C. **Color optical flow**. In: Workshop on digital image computing, volume 1, p. 135–139. Australian Pattern Recognition Society, 2003.

[4] Augereau, B.; Tremblais, B. ; Fernandez-Maloigne, C. **Vectorial Computation of the Optical Flow in Color Image Sequences**. In: Thirteenth Color Imaging Conference, volume 13, p. 130–134, Scottsdale, United States, Nov. 2005. http://www.imaging.org/store/epub.cfm?abstrid=33533.

[5] Baker, S.; Scharstein, D.; Lewis, J.; Roth, S.; Black, M. J. ; Szeliski, R. A database and evaluation methodology for optical flow. **International Journal of Computer Vision**, v.92, n.1, p. 1–31, 2011.

[6] Baker, S.; Scharstein, D.; Lewis, J.; Roth, S.; Black, M. J. ; Szeliski, R. **A database and evaluation methodology for optical flow**. In: Computer Vision, 2007. ICCV 2007. IEEE 11th International Conference on, p. 1–8. IEEE, 2007.

[7] Barron, J.; Klette, R. **Quantitative color optical flow**. In: Pattern Recognition, 2002. Proceedings. 16th International Conference on, volume 4, p. 251–255. IEEE, 2002.

[8] Barron, J. L.; Fleet, D. J. ; Beauchemin, S. Performance of optical flow techniques. **International journal of computer vision**, v.12, n.1, p. 43–77, 1994.

[9] Beauchemin, S. S.; Barron, J. L. The computation of optical flow. **ACM Computing Surveys (CSUR)**, v.27, n.3, p. 433–466, 1995.

[10] Black, M. J.; Anandan, P. The robust estimation of multiple motions: Parametric and piecewise-smooth flow fields. **Computer vision and image understanding**, v.63, n.1, p. 75–104, 1996.

[11] Brox, T.; Bruhn, A.; Papenberg, N. ; Weickert, J. **High accuracy optical flow estimation based on a theory for warping**. In: Computer Vision-ECCV 2004, p. 25–36. Springer, 2004.

[12] Fleet, D. J.; Jepson, A. D. Computation of component image velocity from local phase information. **International Journal of Computer Vision**, v.5, n.1, p. 77–104, 1990.

[13] Golland, P.; Bruckstein, A. M. Motion from color. **Computer Vision and Image Understanding**, v.68, n.3, p. 346–362, 1997.

[14] Gupta, S. N.; Prince, J. L. Stochastic models for div-curl optical flow methods. **Signal Processing Letters, IEEE**, v.3, n.2, p. 32–34, 1996.

[15] Heeger, D. J. Optical flow using spatiotemporal filters. **International Journal of Computer Vision**, v.1, n.4, p. 279–302, 1988.

[16] Horn, B. K.; Schunck, B. G. Determining optical flow. **Artificial intelligence**, v.17, n.1, p. 185–203, 1981.

[17] Lei, C.; Yang, Y.-H. **Optical flow estimation on coarse-to-fine region-trees using discrete optimization**. In: Computer Vision, 2009 IEEE 12th International Conference on, p. 1562–1569. IEEE, 2009.

[18] Lempitsky, V.; Roth, S. ; Rother, C. **Fusionflow: Discrete-continuous optimization for optical flow estimation**. In: Computer Vision and Pattern Recognition, 2008. CVPR 2008. IEEE Conference on, p. 1–8. IEEE, 2008.

[19] Li, Y.; Huttenlocher, D. P. **Learning for optical flow using stochastic optimization**. In: Computer Vision–ECCV 2008, p. 379–391. Springer, 2008.

[20] Lucas, B. D.; Kanade, T. ; others. **An iterative image registration technique with an application to stereo vision**. In: Proceedings of the 7th international joint conference on Artificial intelligence, 1981.

[21] Liu, C.; Yuen, J.; Torralba, A.; Sivic, J. ; Freeman, W. T. **Sift flow: dense correspondence across different scenes**. In: Computer Vision–ECCV 2008, p. 28–42. Springer, 2008.

[22] Markandey, V.; Flinchbaugh, B. E. **Multispectral constraints for optical flow computation**. In: Computer Vision, 1990. Proceedings, Third International Conference on, p. 38–41. IEEE, 1990.

[23] Mota, V.; Perez, E.; Vieira, M.; Maciel, L.; Precioso, F. ; Gosselin, P. **A tensor based on optical flow for global description of motion in videos**. In: Graphics, Patterns and Images (SIBGRAPI), 2012 25th SIBGRAPI Conference on, p. 298–301, 2012.

[24] Nagel, H.-H. On the estimation of optical flow: Relations between different approaches and some new results. **Artificial intelligence**, v.33, n.3, p. 299–324, 1987.

[25] OHTA, N. Optical flow detection by color images. **NEC research & development**, , n.97, p. 78–84, 1990.

[26] O'Donovan, P. **Optical flow: Techniques and applications**, 2005.

[27] Pratt, W. K. Correlation techniques of image registration. **Aerospace and Electronic Systems, IEEE Transactions on**, , n.3, p. 353–358, 1974.

[28] Rannacher, J. Realtime 3d motion estimation on graphics hardware. **Undergraduate Thesis, Heidelberg University**, 2009.

[29] Seitz, S. M.; Baker, S. **Filter flow**. In: Computer Vision, 2009 IEEE 12th International Conference on, p. 143–150. IEEE, 2009.

[30] Sun, D.; Roth, S.; Lewis, J. ; Black, M. J. **Learning optical flow**. In: Computer Vision–ECCV 2008, p. 83–97. Springer, 2008.

[31] Tao, M.; Bai, J.; Kohli, P. ; Paris, S. **Simpleflow: A non-iterative, sublinear optical flow algorithm**. In: Computer Graphics Forum, volume 31, p. 345–353. Wiley Online Library, 2012.

[32] Tschumperlé, D. **Pdes based regularization of multivalued images and applications**, 2002.

[33] Waxman, A. M.; Wu, J. ; Bergholm, F. **Convected activation profiles and the measurement of visual motion**. In: Computer Vision and Pattern Recognition, 1988. Proceedings CVPR'88., Computer Society Conference on, p. 717–723. IEEE, 1988.

[34] Wedel, A.; Pock, T.; Zach, C.; Bischof, H. ; Cremers, D. **An improved algorithm for tv-l 1 optical flow**. In: Statistical and Geometrical Approaches to Visual Motion Analysis, p. 23–45. Springer, 2009.

[35] Xu, L.; Chen, J. ; Jia, J. **A segmentation based variational model for accurate optical flow estimation**. In: Computer Vision–ECCV 2008, p. 671–684. Springer, 2008.

[36] Xu, L.; Dai, Z. ; Jia, J. **Scale invariant optical flow**. In: Computer Vision–ECCV 2012, p. 385–399. Springer, 2012.

[37] Zimmer, H.; Bruhn, A.; Weickert, J.; Valgaerts, L.; Salgado, A.; Rosenhahn, B. ; Seidel, H.-P. **Complementary optic flow**. In: Energy minimization methods in computer vision and pattern recognition, p. 207–220. Springer, 2009.

[38] van de Weijer, J.; Gevers, T. **Robust optical flow from photometric invariants**. In: Image Processing, 2004. ICIP'04. 2004 International Conference on, volume 3, p. 1835–1838. IEEE, 2004.